

# In-situ high spatial resolution LA-MC-ICPMS $^{230}\text{Th}/\text{U}$ dating enables detection of small-scale age inversions in speleothems

Yiming Lin <sup>a</sup>, Klaus Peter Jochum <sup>a,b,\*</sup>, Denis Scholz <sup>c</sup>, Dirk L. Hoffmann <sup>d</sup>, Brigitte Stoll <sup>a,b</sup>,  
Ulrike Weis <sup>a,b</sup>, Meinrat O. Andreae <sup>a,e</sup>

<sup>a</sup> Biogeochemistry Department, Max Planck Institute for Chemistry, P.O. Box 3060, 55020 Mainz, Germany

<sup>b</sup> Climate Geochemistry Department, Max Planck Institute for Chemistry, P.O. Box 3060, 55020 Mainz, Germany

<sup>c</sup> Institute for Geosciences, University of Mainz, 55099 Mainz, Germany

<sup>d</sup> Department of Human Evolution, Max Planck Institute for Evolutionary Anthropology, Deutscher Platz 6, 04103 Leipzig, Germany

<sup>e</sup> Geology and Geophysics Department, King Saud University, Riyadh, Saudi Arabia

Received 23 August 2016; revised 20 December 2016; accepted 30 December 2016

Available online ■■■

## Abstract

We present an in-situ method for Th and U isotope measurements by laser ablation multi-collector inductively coupled plasma mass spectrometry (LA-MC-ICPMS) to determine possible age inversions of stalagmites, using a 213 nm Nd:YAG laser connected to an MC-ICPMS. Due to the low ion beam intensity of  $^{230}\text{Th}$  (20–120 counts per second, cps), we carefully optimized the operating parameters to get highest possible ion beam intensities, i.e., laser fluence ( $25 \text{ J cm}^{-2}$ ), spot size ( $110 \mu\text{m}$ ), pulse repetition rate (20 Hz), scan speed ( $4 \mu\text{m s}^{-1}$ ), integration time (1000 s), and He and Ar gas flow ( $\sim 0.9 \text{ L min}^{-1}$  and  $\sim 0.6 \text{ L min}^{-1}$  respectively). A precision (2 relative standard error, 2RSE) of better than 1.8% was obtained for a single  $^{230}\text{Th}/^{238}\text{U}$  measurement performed on a stalagmite from Hüttenbläuserschachthöhle, western Germany, having U concentrations of  $2\text{--}7 \mu\text{g g}^{-1}$  and with  $^{230}\text{Th}$  beam intensity of less than 100 cps. Compared to previous studies (Hoffmann et al., 2009), this is the about same precision, however at lower U concentrations. The data are corrected and calibrated by two factors ( $F_1$  and  $F_2$ ) for  $^{230}\text{Th}/^{238}\text{U}$  and  $^{234}\text{U}/^{238}\text{U}$ , respectively, using a carbonate material (flowstone in secular equilibrium). We obtained an age uncertainty (2 SE,  $2\sigma$ ) of ca. 9 ka at ca. 215 ka. Most data agree with solution MC-ICPMS results obtained on the same sample within their uncertainties. The reproducibility of the LA-MC-ICPMS age data is within 4.5% (2RSE) as determined from 3 to 4 repeated analyses. With a spot size of  $110 \mu\text{m}$  and spatial resolution of about  $400 \mu\text{m}$  or higher, it is possible to see much more details in thin growing layers than conventional solution analysis, where mixed layer sampling cannot be avoided. Potential age inversions in small regions are revealed, which cannot be detected by solution analysis due to the insufficient spatial resolution.

Copyright © 2017, Guangzhou Institute of Geochemistry. Production and hosting by Elsevier B.V. This is an open access article under the CC BY-NC-ND license (<http://creativecommons.org/licenses/by-nc-nd/4.0/>).

**Keywords:** Laser ablation; MC-ICPMS;  $^{230}\text{Th}/\text{U}$  dating; Speleothem

## 1. Introduction

$^{230}\text{Th}/\text{U}$  dating of speleothems using highly precise and accurate state-of-the-art analytical methods, such as solution-

based multi-collector inductively coupled plasma mass spectrometry (MC-ICPMS) has demonstrated the possibility of age inversions, i.e., the ages do not increase with increasing distance from top as expected from the stratigraphy (Dutton et al., 2009; Hoffmann et al., 2010; Lachniet et al., 2012; Scholz and Hoffmann, 2011; Scholz et al., 2012, 2014; Tolzmann, 2013). In this case, the ages scatter along the growth axis showing both younger and older ages than expected. A potential reason for such age inversions is a so-called open system, i.e., mainly

\* Corresponding author. Climate Geochemistry Department, Max Planck Institute for Chemistry, P.O. Box 3060, 55020 Mainz, Germany.

E-mail address: [k.jochum@mpic.de](mailto:k.jochum@mpic.de) (K.P. Jochum).

Peer review under responsibility of Guangzhou Institute of Geochemistry.

<http://dx.doi.org/10.1016/j.sesci.2016.12.003>

2451-912X/Copyright © 2017, Guangzhou Institute of Geochemistry. Production and hosting by Elsevier B.V. This is an open access article under the CC BY-NC-ND license (<http://creativecommons.org/licenses/by-nc-nd/4.0/>).

Please cite this article in press as: Lin, Y., et al., In-situ high spatial resolution LA-MC-ICPMS  $^{230}\text{Th}/\text{U}$  dating enables detection of small-scale age inversions in speleothems, Solid Earth Sciences (2017), <http://dx.doi.org/10.1016/j.sesci.2016.12.003>

loss or addition of U after deposition, which will lead to altered  $^{230}\text{Th}/\text{U}$  ages. Due to the limited spatial resolution of conventional solution MC-ICPMS, detection of small-scale age inversions may be impossible (Scholz et al., 2014). Micromilling significantly helps to improve spatial resolution (Hoffmann et al., 2009). Information at high spatial resolution using LA-MC-ICPMS may be important, for instance to date rapid, short-term climate oscillations observed in a speleothem proxy record. Furthermore, the temporal resolution of palaeoclimate proxy records depends on the growth rate of the speleothem. Thus, for slowly growing speleothems, the timing and duration of climate events can only be precisely determined if high spatial resolution dating is possible (Hoffmann et al., 2009). In-situ microanalytical methods have been presented for  $^{230}\text{Th}/\text{U}$  dating by using secondary ionization mass spectrometry (SIMS) (Bacon et al., 2000; Reid et al., 1997), laser ablation (LA)-MC-ICPMS (Eggins et al., 2005; Hoffmann et al., 2009; Potter et al., 2005; Stirling et al., 2000), and micromilling combined with MC-ICPMS (Drysdale et al., 2012; Hoffmann et al., 2009). SIMS has a high spatial resolution, however it suffers from severe matrix effects (Sodhi, 2004). Notably, LA-MC-ICPMS offers a new dimension of applications in Earth sciences with rapidly increasing use, for instance for isotopic measurements (Hf, Sr, Pb ...) and U–Pb dating (Iizuka and Hirata, 2005; Jackson et al., 2001; Paul et al., 2011; Waight et al., 2002). Although precision and sensitivity are reduced compared to conventional solution analysis, highly spatially resolved ( $<100\ \mu\text{m}$ ) measurement can be achieved by LA-MC-ICPMS. In general, two main difficulties limit LA measurement of U-series isotopes in carbonate samples, such as speleothems. The first is the low U concentration ( $\sim 1\ \mu\text{g g}^{-1}$  or lower) of most natural samples and the very low abundance of  $^{230}\text{Th}$ , which in turn depends on the U concentration. The second is the difficulty to get reliable matrix-matched external calibration materials with high U concentration and homogeneous known ( $^{230}\text{Th}/^{238}\text{U}$ ) and ( $^{234}\text{U}/^{238}\text{U}$ ) ratios. Only few studies have systematically applied LA-MC-ICPMS for in-situ  $^{230}\text{Th}/\text{U}$  dating of speleothems (Eggins et al., 2005; Hellstrom, 2003; Hoffmann et al., 2009). However, most of the previous studies have not focused on the investigation of small-scale age inversions.

The aim of this paper is to apply the LA-MC-ICPMS method to precisely and accurately measure U-series isotope ratios in stalagmites and investigate the potential to detect small-scale age inversions.

## 2. Material and methods

### 2.1. Samples

Stalagmite HBSH-1 stems from the Hüttenblärschachhöhle, western Germany (Yang et al., 2015). Fig. 1 shows a picture of HBSH-1, which is approximately 55 cm long and shows a clearly visible lamination. The stalagmite is mainly composed of aragonite, as has been revealed by X-ray diffraction analysis. A previous study has shown relatively

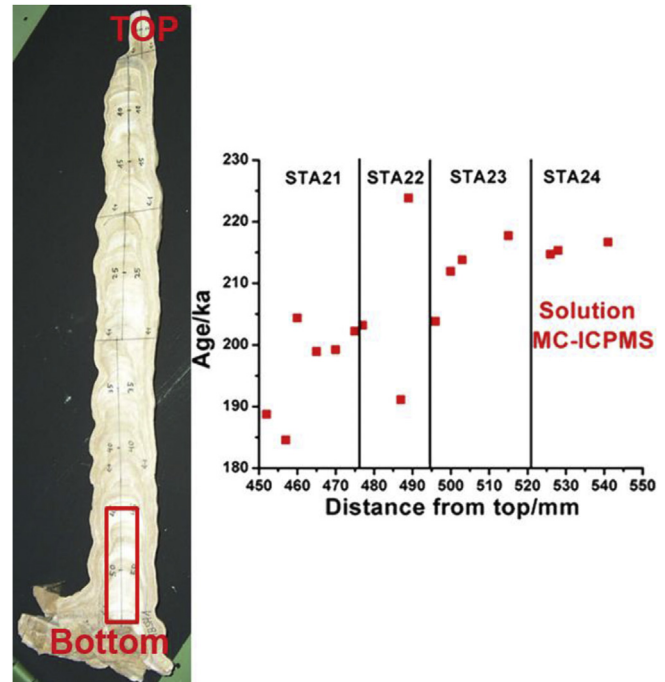


Fig. 1. Picture of stalagmite HBSH-1 from the Hüttenblärschachhöhle, western Germany.  $^{230}\text{Th}/\text{U}$ -ages (Scholz et al., unpublished) were obtained by solution MC-ICPMS. The section investigated in this study ranges from 450 to 543 mm dft, and four available pieces are indicated by the red rectangle.

high concentrations of several trace elements, such as Pb, Ba, Sr, and U, in the aragonite phase (Jochum et al., 2012). A high U content is beneficial for in-situ  $^{230}\text{Th}/\text{U}$  dating, because ion beam intensities directly depend on the U concentration. The area we investigated is a small part between 450 and 543 mm distance from top (dft) indicated by the red frame in Fig. 1. Previous  $^{230}\text{Th}/\text{U}$  ages were obtained from solution MC-ICPMS analyses by Scholz and Hoffmann (2016) (red dots) and Yang et al. (2015) (black dots). The age differences between the two solution results may be due to the different sampling positions, although they were taken at the same distance from top. For comparison, we use the results of Scholz and Hoffmann (2016), because the sampling positions are more close to those of the laser ablation (LA) measurements. Even in such small areas, the growing conditions can be quite different. Four pieces are available for investigation: STA24 (521.2–542.8 mm dft) is a fast-growing section, which shows similar ages for the whole section; STA23 (494.75–521.15 mm dft) is a relative slowly growing section with increasing ages from top to bottom layers. Solution MC-ICPMS analysis shows age inversions within sections STA22 (476.3–494.7 mm dft) and STA21 (450.05–476.25 mm dft) (Fig. 1). Typical U and Th concentrations of HBSH-1 are 2–7 and  $0.001\text{--}1\ \mu\text{g g}^{-1}$ , respectively (Fig. 2). The trace elements were measured using an Element 2 single-collector ICPMS coupled to a laser ablation system (see below). A detailed description of the methodology and the analytical protocol is given by Jochum et al. (2012).

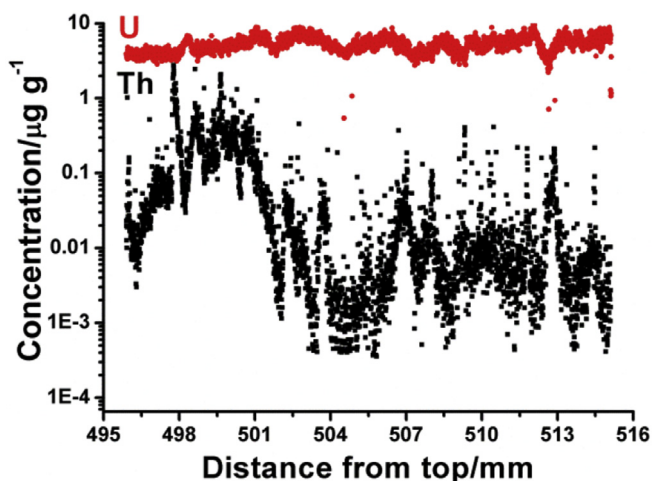


Fig. 2. Evolution of the U and Th concentration in section STA23. The other pieces have the same levels of U and Th concentrations, which are not shown here.

## 2.2. Laser ablation

LA sampling was performed with a 213 nm Nd:YAG laser (UP-213, New Wave Research, Inc., Fremont, CA, USA) at the Max Planck Institute for Chemistry (MPIC), Mainz, Germany. It was carried out in a New Wave Large Format Cell (15 × 15 cm) in a He atmosphere enabling the analysis of large samples. The ablated particles were mixed with an Ar gas flow before introduction to the plasma (Table 1). The uncertainty of age determination is limited by the low

Table 1

Collector configuration of Nu Plasma MC-ICPMS with isotopes monitored. Ax: central Faraday cup; H: Faraday cup at high mass side; L: Faraday cup a low mass side; IC: ion counter.

	H1	Ax	L1	L2	IC0	L3	IC1	L4	IC2
Zero 1	237.5			234.5	233.5		231.5		229.5
Cycle 1	<sup>238</sup> U			<sup>235</sup> U	<sup>234</sup> U		<sup>232</sup> Th		<sup>230</sup> Th

abundance of <sup>230</sup>Th, which can be improved by optimizing the sensitivity of Th. The highest ablation output is necessary to get the optimal <sup>230</sup>Th signal intensity, which includes largest spot size (110 μm), and maximum fluence and pulse repetition (20 Hz) of the UP-213 laser (Fig. 3). Maximum count rates of about 80–120 and 50–80 cps were obtained for stalagmite HBSH-1 and flowstone WM 1 samples, respectively. In addition to these parameters, line scan mode was used to obtain a constant ion beam (Koornneef et al., 2012). The scan rate is important as well, because too slow or too fast scan speeds would deteriorate the ion beam intensity and therefore the precision (Mertz-Kraus et al., 2010). A scan rate of 2–10 μm s<sup>-1</sup> was found to be optimal, and in this study we used 4 μm s<sup>-1</sup>. With an overall ablation time of 1000 s, a laser track of 4 mm length and about 50 μm depth was used, corresponding to an ablated material of about 60 μg (Fig. 5).

Instrumental tuning and parameter optimization were performed with the homogeneous reference glass NIST SRM 610 containing high concentrations of U and Th (ca. 400 μg g<sup>-1</sup>) (Jochum et al., 2011). The high yields of ion beam intensities facilitate instrumental tuning procedures. The transport efficiency of the ablated particles strongly depends on the helium–argon mixture used as aerosol carrier (Günther and Heinrich, 1999; Koornneef et al., 2012). Fig. 4 shows the influence of He and Ar gas flows on the <sup>232</sup>Th signal intensity tested on NIST SRM 610. The best sensitivity of Th can only be reached with specific combinations of the two gas flows. High He gas flow requires low Ar gas flow and vice versa. Different combinations resulted in similar maximum <sup>232</sup>Th intensities (~2.0 V). However, gas flows at extreme conditions will deteriorate the signal stability. The He and Ar gas flows used here are ~0.9 and ~0.6 L min<sup>-1</sup>, respectively, where the minimum elemental fractionation of Th and U was observed as well. Although NIST SRM 610 was used, we also checked the speleothem samples for tuning the parameters and observed no significant difference between the silicate glass and carbonate samples. Table 2 shows the typical operating parameters used in this study.

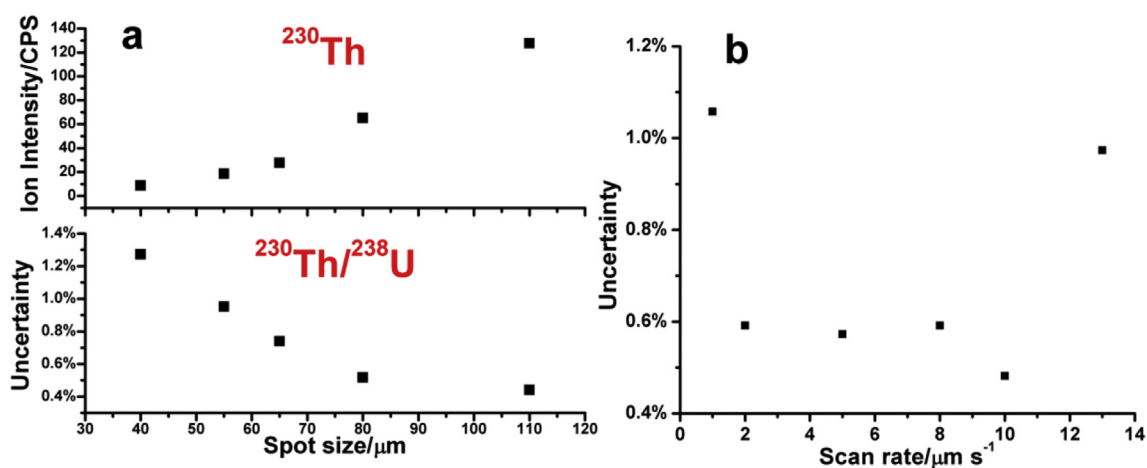


Fig. 3. Dependence of the <sup>230</sup>Th signal intensity and the uncertainty (RSE) of <sup>230</sup>Th/<sup>238</sup>U on (a) laser spot size and (b) scan rate. Number of mass spectrometric cycles: N = 100.



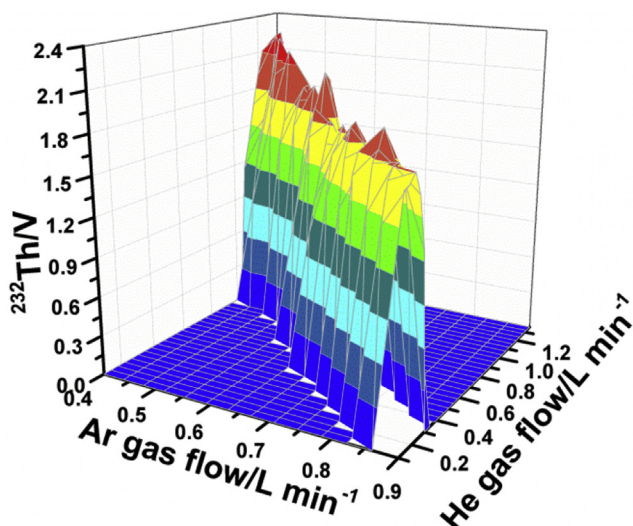


Fig. 4. Influence of He and Ar gas flows on the signal intensity of  $^{232}\text{Th}$  tested on NIST SRM 610. High He gas flow requires low Ar gas flow and vice versa to reach the best sensitivity for Th. Similar  $^{232}\text{Th}$  signal intensities ( $\sim 2.0$  W) can be optimized using different combinations of the two gas flows.

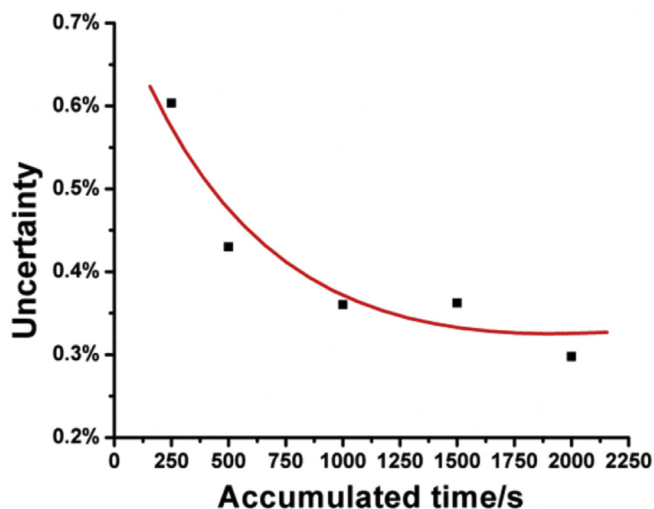


Fig. 5. Dependence of the analytical precision of  $^{230}\text{Th}/^{238}\text{U}$  on the integration time tested on section STA24. The heterogeneity of the elemental distribution in speleothem samples and instrumental dark noise does affect the precision.

As calibration material, we used the flowstone sample WM 1 from Wilder Mann Cave, which is located in the Northern Calcareous Alps (NCA) close to the Austrian-German border (Meyer et al., 2009, 2011). WM 1 has been shown to be in secular equilibrium (Cheng et al., 2013; Hoffmann et al., 2007). Uranium is heterogeneously distributed in this sample with concentrations varying between 3 and  $15 \mu\text{g g}^{-1}$ . The Th concentration is negligibly low ( $<0.1 \mu\text{g g}^{-1}$ ). The flowstone sample is an ideal external standard because it has the same matrix as well as similar U and Th concentrations as the HBSH-1 sample. Moreover, the activity ratios of interest are known and uniform in the sample. Prior to analysis, all samples were polished and cleaned with ethanol and then mounted in the ablation cell by epoxy resin. Preablation was always carried

Table 2  
Operating parameters used for stalagmite age dating.

ICPMS	Nu plasma multi-collector
RF power/W	1300
Cool gas flow rate/ $\text{l min}^{-1}$	15
Auxiliary gas flow rate/ $\text{l min}^{-1}$	1
Carrier gas (Ar) flow rate/ $\text{l min}^{-1}$	0.6
Carrier gas (He) flow rate/ $\text{l min}^{-1}$	0.9
<b>Laser</b>	<b>New Wave UP 213 laser ablation system</b>
Wavelength/nm	213
Pulse duration/ns	5
Repetition rate/Hz	20
Fluence/ $\text{J cm}^{-2}$	10
Spot size/ $\mu\text{m}$	110
Scan speed/ $\mu\text{m s}^{-1}$	4
<b>Data acquisition parameters</b>	
Integration time per cycle/s	10
Gas blank time/s	20
Total integration time/s	1000

out prior to actual data acquisition using a fast scan speed to remove surface contamination. The carbonate can be polished to remove the ablation track in the surface for repeated analysis.

### 2.3. MC-ICPMS

The Nu Plasma MC-ICPMS (Nu Instruments, Wrexham) at the MPIC, Mainz, is equipped with 12 Faraday cups and 3 ion counting detectors. The collector configuration and analytical routines used in this study are shown in Table 1. The low-abundance isotopes of interest ( $^{234}\text{U}$  and  $^{230}\text{Th}$ ) were measured on ion counting detectors. U and Th isotopes were analyzed simultaneously in one cycle. Prior to all analyses, one cycle with the beam deflected (Zero 1) was performed to determine ablation background. A typical value for  $^{230}\text{Th}$  is 0.1 cps.

Abundance sensitivity of  $^{238}\text{U}$  at mass 234 determined at the half masses 233.5 and 234.5 was about  $5 \times 10^{-7}$ , which corresponds to a contribution of 6‰ from the  $^{238}\text{U}$  tail. The equivalent effect is assumed for reference materials and unknowns, and the associated error on the corrected  $^{234}\text{U}/^{238}\text{U}$  ratio is neglected. Tail contribution of  $^{232}\text{Th}$  onto  $^{230}\text{Th}$  was insignificant in most cases. In some positions, the  $^{232}\text{Th}$  concentration was higher than  $0.5 \mu\text{g g}^{-1}$  (Fig. 2) and the tail contribution to  $^{230}\text{Th}$  will be significant. The LA line scans and measurements on such difficult positions were avoided. As a consequence a potential correction for contamination by detrital  $^{230}\text{Th}$  is insignificant. Thus the influence of peak tailing can be ignored, reducing the time consumed for peak jumping. Drift of mass bias, Faraday cup to ion counter gain, and different sensitivity factors for U and Th were monitored and determined by standard bracketing.

### 2.4. Data reduction and uncertainty

First, the raw ratios were corrected for the background. Then, data correction is conducted by two correction factors,  $F_1$  and  $F_2$ , which are defined as follows:

$$F_1 = \frac{\left(\frac{^{230}\text{Th}}{^{238}\text{U}}\right)_{\text{meas}}}{\left(\frac{^{230}\text{Th}}{^{238}\text{U}}\right)_{\text{true}}} \quad (1)$$

$$F_2 = \frac{\left(\frac{^{234}\text{U}}{^{238}\text{U}}\right)_{\text{meas}}}{\left(\frac{^{234}\text{U}}{^{238}\text{U}}\right)_{\text{true}}} \quad (2)$$

where  $(^{230}\text{Th}/^{238}\text{U})_{\text{meas}}$ ,  $(^{230}\text{Th}/^{238}\text{U})_{\text{true}}$ ,  $(^{234}\text{U}/^{238}\text{U})_{\text{meas}}$  and  $(^{234}\text{U}/^{238}\text{U})_{\text{true}}$  are the measured and the “true” activity ratios respectively.  $F_1$  and  $F_2$  were obtained from the flowstone sample WM1 during standard bracketing analysis. The unknown ratios for the stalagmite samples in between are then corrected using a factor derived by linear interpolation of bracketing values for  $F_1$  and  $F_2$ . This correction strategy provides a quick and simple correction, where  $F_1$  includes the corrections of mass bias, different sensitivity factors between Th and U, as well as Faraday cup to ion counter gain of IC2; Similarly,  $F_2$  includes corrections of mass bias and Faraday cup to ion counter gain of IC0. Ion counter nonlinearity effects are small compared to the main sources of uncertainties like statistical uncertainty due to the low count rate (see below) and hence were assumed to be negligible. This simplified protocol is effective by combining all corrections in a single correction factor and can be used if all samples have similar compositions. If this is not the case, a more detailed protocol is recommended (Hoffmann et al., 2007).

The uncertainty is mainly dominated by the precision of the measured activity ratios. On the other hand, the uncertainties of the correction factors  $F_1$  and  $F_2$  are also propagated to the linear ratio corrections, which are based on the following equations:

$$\left(\frac{^{230}\text{Th}}{^{238}\text{U}}\right)_{\text{true}} = \left(\frac{^{230}\text{Th}}{^{238}\text{U}}\right)_{\text{meas}} * 2 / (F_1 + F'_1) \quad (3)$$

$$\left(\frac{^{234}\text{U}}{^{238}\text{U}}\right)_{\text{true}} = \left(\frac{^{234}\text{U}}{^{238}\text{U}}\right)_{\text{meas}} * 2 / (F_2 + F'_2) \quad (4)$$

For instance, for  $(^{230}\text{Th}/^{238}\text{U})$ ,  $F_1$  and  $F'_1$  are two correction factors obtained from the calibration material during bracketing analysis. The combined analytical uncertainty follows the rule of error propagation:

$$u_{\text{total}} = \sqrt{u_{\text{meas}}^2 + (0.5u_{F_1})^2 + (0.5u_{F'_1})^2 + u_{\text{add}}^2} \quad (5)$$

where the uncertainties of  $F_1$  (i.e.,  $u_{F_1}$ ),  $F'_1$  ( $u_{F'_1}$ ) and the measured stalagmite activity ratio ( $u_{\text{meas}}$ ) represent the major contributions to the total uncertainty ( $u_{\text{total}}$ ) of corrected  $(^{230}\text{Th}/^{238}\text{U})$ . The uncertainty of  $(^{234}\text{U}/^{238}\text{U})$  is calculated analogously. Additional uncertainties ( $u_{\text{add}}$ ) are the minor components, which may include the counting statistics of the isotope ratios, tailing corrections, uncertainties of half lives, the “true” activity ratios of flowstone WM 1 and others (Mertz-Kraus et al., 2010).  $u_{\text{add}}$  is  $< 1-2\%$ . The uncertainties of both corrected  $(^{230}\text{Th}/^{238}\text{U})$  and  $(^{234}\text{U}/^{238}\text{U})$  are propagated to the final age uncertainty, which is calculated by Monte-

Carlo simulation (Ludwig, 2003). The detection limit for the age determination depends on various parameters, such as the count rate of  $^{230}\text{Th}$ , the U concentration and the initial  $(^{234}\text{U}/^{238}\text{U})$  activity ratio. Therefore, age limitation is difficult to quantify. The higher the U concentration and initial  $(^{234}\text{U}/^{238}\text{U})$ , the better the minimum age can be determined.

### 3. Results and discussion

#### 3.1. Reliability of in-situ $^{230}\text{Th}/\text{U}$ dating

The solution MC-ICPMS data (Fig. 1) show that section STA24 was relatively fast growing ( $>10 \text{ mm ka}^{-1}$ ) with age differences smaller than 2 ka on 21.6 mm. This section is therefore useful to check our data reduction and correction of LA-MC-ICPMS analysis. Fig. 6 shows the uncorrected and corrected activity ratios of  $(^{234}\text{U}/^{238}\text{U})$  against  $(^{230}\text{Th}/^{238}\text{U})$  for six replicate measurements. Due to the different sensitivities of Th and U, the uncorrected and corrected values show a relatively large difference for  $(^{230}\text{Th}/^{238}\text{U})$ . The LA data points cluster together because the laser sampling lines of about several mm on the sample are close to each other (about 200  $\mu\text{m}$ ) and the positions are different from those of solution analysis. In principle,  $(^{234}\text{U}/^{238}\text{U})$  against  $(^{230}\text{Th}/^{238}\text{U})$  should be linearly correlated for a system of the same age (Hoffmann et al., 2009), which is indicated by the red line in Fig. 6, which is based on the solution MC-ICPMS values. After correction, the LA data are very close to or on the linear correlation line, which confirms the reliability of our correction method. Fig. 7 and Table 3 highlight the reliability by showing a comparison of LA-MC-ICPMS data with the solution MC-ICPMS. The grey band in Fig. 7 shows the age interval from solution MC-

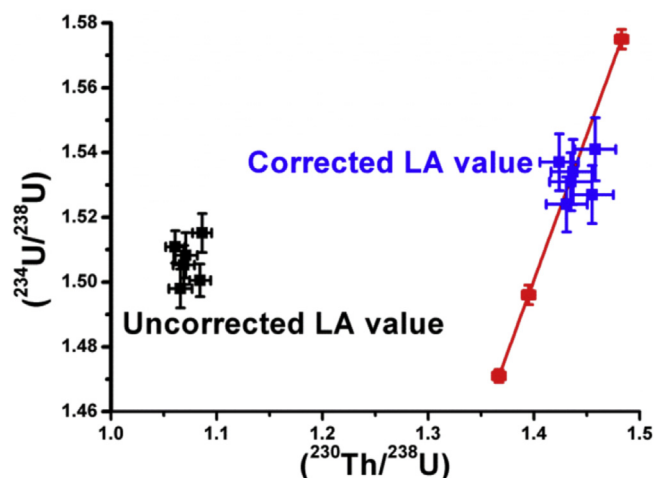


Fig. 6. Raw and corrected LA-MC-ICPMS  $(^{234}\text{U}/^{238}\text{U})$  against  $(^{230}\text{Th}/^{238}\text{U})$  for section STA24. The corrected values were obtained using  $F_1$  and  $F_2$  from flowstone WM 1 as explained in detail in the text. Black squares: uncorrected LA-MC-ICPMS values; blue squares: corrected LA-MC-ICPMS values; red squares: solution MC-ICPMS values. Error bar shows  $2\sigma$ -uncertainties. The error bars of the uncorrected LA values only include the analytical uncertainty. The error bars of the corrected LA values also include the propagated uncertainty of  $F_1$  and  $F_2$ . Red line: theoretical relation of activity ratios based on the solution MC-ICPMS ages.

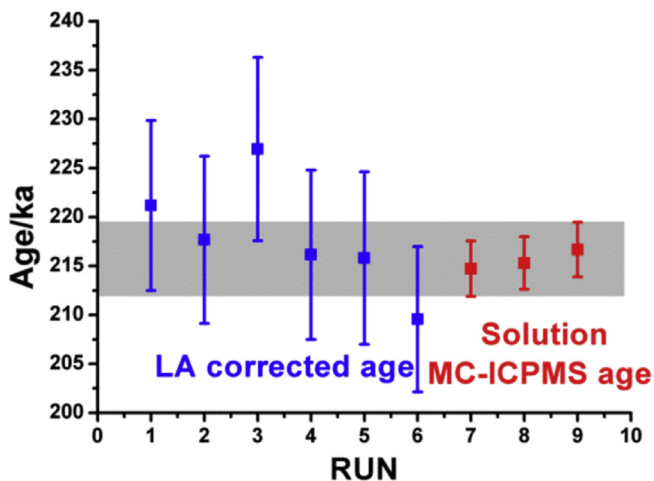


Fig. 7. LA-MC-ICPMS  $^{230}\text{Th}/\text{U}$ -ages compared with the corresponding solution MC-ICPMS ages for section STA24. Blue squares: corrected LA ages; red squares: solution MC-ICPMS ages. Error bars are shown at the  $2\sigma$ -level. The grey band shows the age interval from solution MC-ICPMS analysis.

Table 3  
U-series results obtained on STA24.

Measurement	$(^{230}\text{Th}/^{238}\text{U} \pm 2\sigma^a)$	$(^{234}\text{U}/^{238}\text{U} \pm 2\sigma)$	Age/ka $\pm 2\sigma$
LA-MC-ICPMS-1	1.458 $\pm$ 0.019	1.541 $\pm$ 0.010	221.2 $\pm$ 8.7
LA-MC-ICPMS-2	1.431 $\pm$ 0.019	1.524 $\pm$ 0.008	217.7 $\pm$ 8.5
LA-MC-ICPMS-3	1.455 $\pm$ 0.020	1.527 $\pm$ 0.009	226.9 $\pm$ 9.4
LA-MC-ICPMS-4	1.435 $\pm$ 0.020	1.531 $\pm$ 0.009	216.1 $\pm$ 8.6
LA-MC-ICPMS-5	1.437 $\pm$ 0.021	1.534 $\pm$ 0.010	215.8 $\pm$ 8.8
LA-MC-ICPMS-6	1.424 $\pm$ 0.018	1.537 $\pm$ 0.009	209.5 $\pm$ 7.4
Solution MC-ICPMS-1	1.367 $\pm$ 0.006	1.471 $\pm$ 0.002	214.7 $\pm$ 2.9
Solution MC-ICPMS-2	1.395 $\pm$ 0.006	1.496 $\pm$ 0.003	215.3 $\pm$ 2.7
Solution MC-ICPMS-3	1.483 $\pm$ 0.006	1.575 $\pm$ 0.003	216.7 $\pm$ 2.8

<sup>a</sup>  $\sigma$  = standard error.

ICPMS analysis of section STA24. Individual age uncertainties of the LA measurements are ca. 9 ka ( $2\sigma$ ) at ca. 215 ka (ca. 4–5%, 2 RSE). The LA data agree with each other and plot in the grey interval band within their uncertainties. The mean age of  $217.9 \pm 4.8$  ka ( $2\sigma$ ) is also in good agreement with the derived mean age of  $215.6 \pm 1.2$  ka ( $2\sigma$ ) from solution MC-ICPMS. This confirms that despite the three times lower precision than for solution analysis, in-situ LA  $^{230}\text{Th}/\text{U}$  dating can be performed at high spatial resolution on speleothem samples and is ideal to reveal potential small scale age inversions.

### 3.2. Detection of age inversions at small scale

For LA sampling, we can design the ablation track to follow individual layers. The growth layers of stalagmites are nearly parallel, and we assume the same age for an individual layer. This is a reasonable assumption considering the growth systematic of speleothems (Kaufmann, 2003; Mühlinghaus et al., 2007). Laser tracks are shown in Fig. 8, where sections STA22 and STA23 are presented. Fig. 8a shows the LA-MC-ICPMS data obtained at locations where solution MC-ICPMS analyses are available. Both data sets agree within

uncertainty except for the data point at 503 mm dft. This may be related to our correction method, which means that repeated analyses need to be performed for reliable results. However, here we mainly attribute this disagreement to two other reasons: Firstly, the sampling positions between the two methods - although obtained at the same dft - are not exactly identical because solution MC-ICPMS data have been obtained from a different part of HBSH-1. Secondly, LA analysis enables high spatial resolution, whereas for conventional solution analysis, the sample size is much higher and mixed layer sampling cannot be avoided. The age information obtained by solution analysis may thus represent an average age of multiple layers. By polishing the sample surface, replicate LA dating of the same layer was carried out, which is presented in Fig. 8b for section STA22 and Fig. 8c for section STA23. The red points show the solution data, which have a much lower spatial resolution, and the other points represent LA measurements. Each position at 1 mm (Fig. 8b) or 400  $\mu\text{m}$  (Fig. 8c) intervals has been dated three to four times, yielding a reproducibility (2RSE) of 1%–4.4%. The evolution of the ages is shown by the grey band in Fig. 8b and c, which is based on the  $2\sigma$  error of the mean ages obtained from 3 to 4 replicate measurements. Section STA22 shows an age inversion between 477 and 487 mm dft based on the solution MC-ICPMS data (red dashed line in Fig. 8b). The age decreases from  $203.2 \pm 2.9$  ka ( $2\sigma$ ) at 477 mm dft to  $191.1 \pm 2.6$  ka ( $2\sigma$ ) at 487 mm dft. This inversion is not clearly visible in the LA data (Fig. 8b). As discussed above, due to the sampling position and spatial resolution, an age difference of up to 15 ka between the two techniques even at the same position (position 489 mm dft in Fig. 8b) cannot be excluded. Thus, it is reasonable that no obvious lower age at 487 mm dft was detected by our LA measurements. However, we find an age inversion between 481 and 483 mm dft, where the age decreases from  $210.4 \pm 8.2$  ka ( $2\sigma$ ) to  $188.3 \pm 3.6$  ka ( $2\sigma$ ). This age difference of ca. 22 ka is larger than our methodological uncertainty, even if it is generally higher than for solution MC-ICPMS. Compared to conventional solution analysis, more details can be resolved with a spatial resolution of  $\sim 400$   $\mu\text{m}$  (Fig. 8c for STA23). The growth conditions of stalagmites at such a small scale may be more complicated as indicated by solution analysis (red dashed line), i.e., ages are younger/older than expected from the stratigraphy. Potential age inversions also occur at 497.2–498.4 and 499.2–500 mm dft of section STA23. The age decreases from  $208.4 \pm 7.5$  ka ( $2\sigma$ ) to  $192.4 \pm 6.1$  ka ( $2\sigma$ ) and from  $222.9 \pm 3.4$  ka ( $2\sigma$ ) to  $205.3 \pm 5.4$  ka ( $2\sigma$ ), respectively. Age inversions occurring at such a small scale cannot be discovered by conventional solution MC-ICPMS analysis.

### 3.3. Potential reasons for age inversions

The basic assumptions of the  $^{230}\text{Th}/\text{U}$  dating method are that the U-series decay system remains closed and that no loss or addition of U and Th isotopes after deposition occurs. However, although speleothems are considered as one of the best suited materials for U-series dating due to their protected



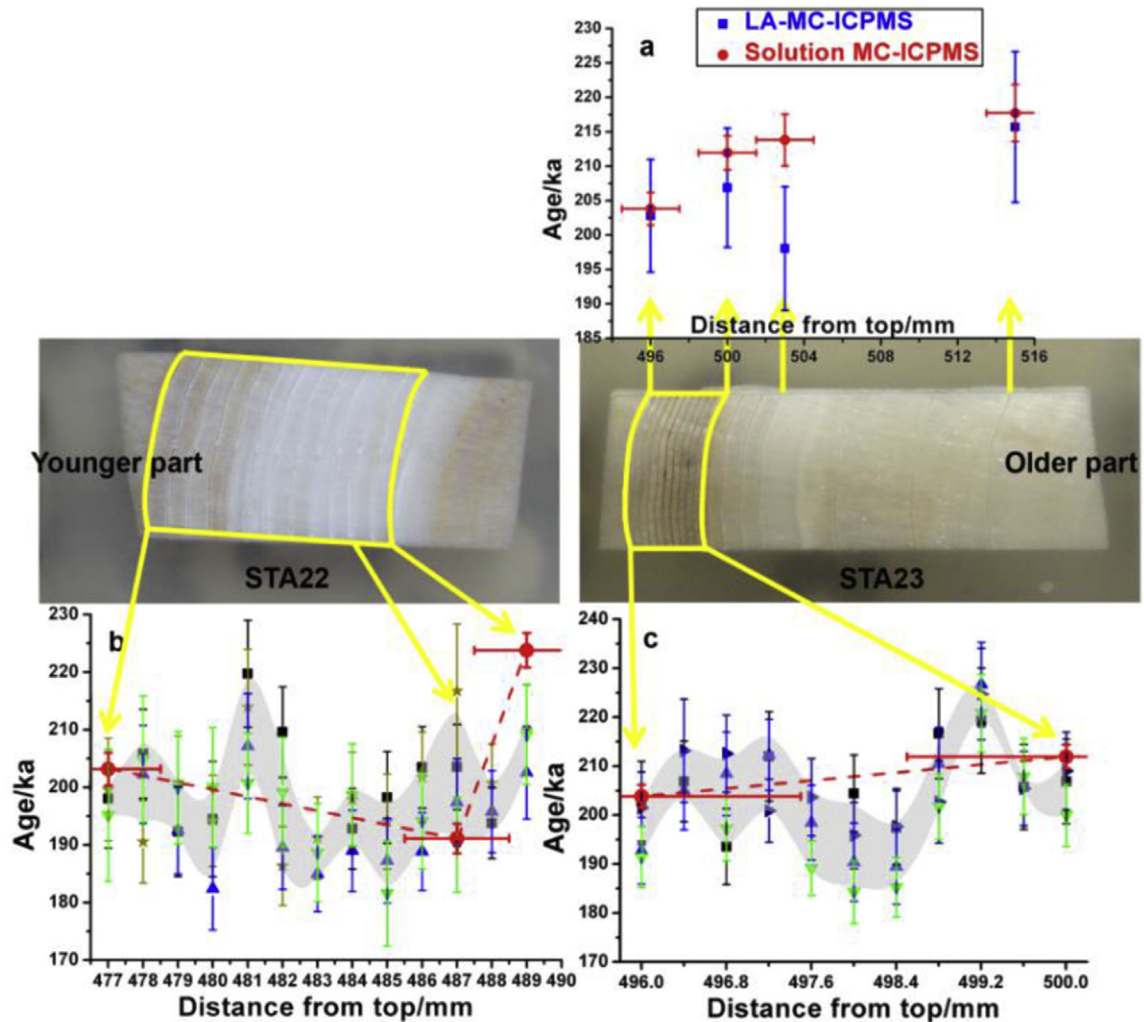


Fig. 8. Curved ablation tracks and corresponding age information for sections STA22 and STA23: a) comparison of LA and solution MC-ICPMS  $^{230}\text{Th}/\text{U}$ -ages for the locations where solution MC-ICPMS data are available for STA23; 3–4 independent LA-MC-ICPMS measurements on b) STA22 and c) STA23 at each distance (black, green, blue symbols). The red points in a), b) and c) are solution MC-ICPMS ages and red dashed lines show simple change of age. The grey bands show the evolution of the ages based on  $2\sigma$ -uncertainty of the mean age of repeated measurements by LA-MC-ICPMS.

growth in caves (Scholz and Hoffmann, 2008), open-system behavior in speleothems has been reported (Borsato et al., 2003). Any process causing loss or addition of U and Th isotopes may lead to altered  $^{230}\text{Th}/\text{U}$  ages. The exact mechanisms causing age inversions may be complex and are not the focus of this paper. For a detailed discussion of the potential processes, the reader is referred to Scholz et al. (2014) or Lachniet et al. (2012), who focus on aragonitic speleothems. Detrital contamination may be one of the important reasons (Borsato et al., 2003; Dorale et al., 2004; Scholz and Hoffmann, 2011). Thorium is commonly associated with detrital material and adsorbed onto particles due to its low solubility. For example, in our HBSH-1 sample, the relationships between LA ages and four important trace elements (U, Th, Mg and P) are shown in Fig. 9. The high intensity of Th in Fig. 9a and the similarity with the P and Mg signal between 497.2 and 498.4 mm dft in section STA23 suggest that the occurrence of these elements is related to incorporation of detrital particles.  $^{230}\text{Th}$  is accompanied by  $^{232}\text{Th}$  and

introduced along with detrital Th, which will lead to higher ( $^{230}\text{Th}/^{238}\text{U}$ ) and thus the older apparent ages. Because elevated  $^{232}\text{Th}$  is avoided, the observed age inversion here (Fig. 9a) is cannot be caused by detrital or initial Th. However, the increase of U concentration from  $\sim 4$  to  $\sim 7 \mu\text{g g}^{-1}$  at 498.4 mm dft may indicate post-depositional mobilization of U (Scholz et al., 2014). U gain or loss may occur during dissolution of previously deposited layers by undersaturated drip water and re-precipitation of speleothem calcium carbonate. Post-depositional addition of U may have a large effect on ( $^{230}\text{Th}/^{238}\text{U}$ ) and will generally lead to lower ( $^{230}\text{Th}/^{238}\text{U}$ ). Thus, younger ages or age inversions can be expected. ( $^{234}\text{U}/^{238}\text{U}$ ) can be affected as well if the ( $^{234}\text{U}/^{238}\text{U}$ ) ratio of the additional U is different from the initial ( $^{234}\text{U}/^{238}\text{U}$ ). U addition may also have happened at  $\sim 482.5$  mm dft of section STA22 although the effect is less pronounced (marked by dashed red line Fig. 9b). The effect of U addition on a  $^{230}\text{Th}/\text{U}$  age depends on the amount of U added and on the timing and duration of the open system (Scholz et al., 2014). Some other

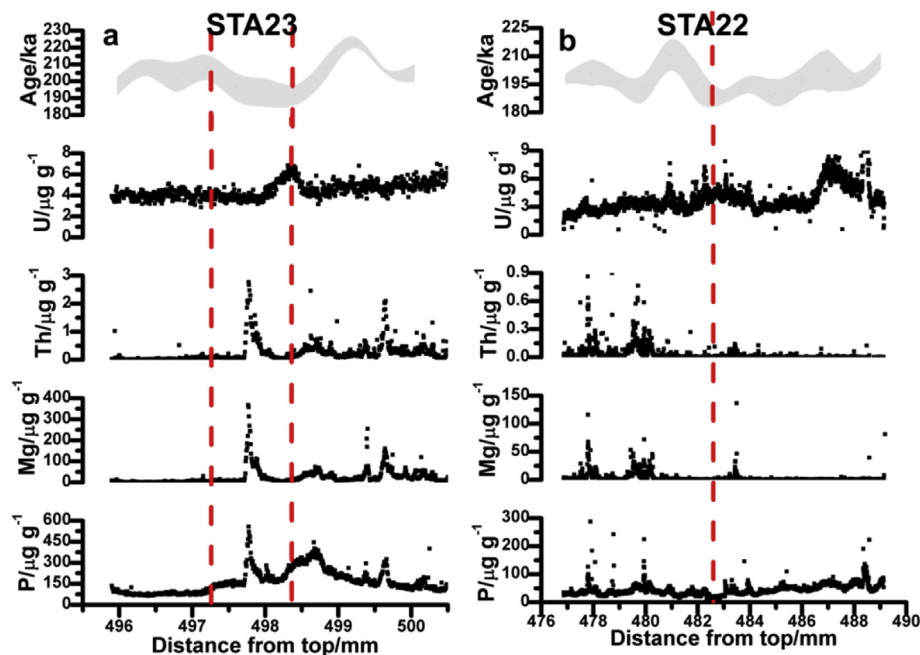


Fig. 9. Comparison of the LA ages with trace element analyses for sections STA23 (a) and STA22 (b). The grey bands are from Fig. 8. The red dashed lines highlight specific regions or points (see text).

diagenetic effects like recrystallization of aragonite will lead to apparently wrong  $^{230}\text{Th}/\text{U}$  ages as well (Frisia et al., 2002; Railsback et al., 2002). Aragonite-to-calcite transformation may result in the loss of U concentration. The mobility of U and Th caused by the diagenetic solutions can be very different due to their solubility. Chemical alteration of ratios by the leaching of U and retention of Th during the recrystallization process will lead to inaccurate calculated  $^{230}\text{Th}/\text{U}$  ages that do not represent real depositional ages.

#### 4. Conclusions

LA-MC-ICPMS  $^{230}\text{Th}/\text{U}$  dating provides significant advantages over traditional solution MC-ICPMS dating: (i) nearly no chemical preparation is required, (ii) rapid analysis, and (iii) high spatial resolution are possible. LA-MC-ICPMS  $^{230}\text{Th}/\text{U}$  dating can be performed for carbonate samples with a U concentration of several  $\mu\text{g g}^{-1}$ . For lower U concentrations and younger ages, the sensitivity related disadvantage would limit the application of LA-MC-ICPMS due to the lower precision and accuracy. In this work, a precision (2RSE) of better than 1.8% was obtained for single  $^{230}\text{Th}/^{238}\text{U}$  measurement with 20–120 cps of  $^{230}\text{Th}$  signal intensity. An internal precision of ca. 9 ka at  $2\sigma$ -level for an age of ca. 215 ka can be achieved. The reproducibility (2RSE) for 3–4 repeated measurements is within 4.5%. Age inversions occurring on a very small scale can be revealed, which is not possible using conventional solution MC-ICPMS analysis. Bracketing carbonate materials with high U concentration, nearly no  $^{232}\text{Th}$ , and well-analyzed isotope ratios (preferably in secular equilibrium) are important for accurate matrix-matched external calibration.

Future instrumental updates which include higher resistance of the amplifier (Trinquier et al., 2013); re-design of the interface system (Cottle et al., 2013), and the use of a femtosecond laser (Jochum et al., 2014) would certainly improve the performance of LA-MC-ICPMS  $^{230}\text{Th}/\text{U}$  dating.

#### Acknowledgements

Y. Lin thanks the Max Planck Institute for Chemistry in Mainz, Germany, for financial support. We also thank D.K. Richter, S. Niggemann and W. Grebe for providing stalagmite HBSH-1. Furthermore, we thank Q. Yang and C. Obert for discussion. This study was funded by the Max Planck Society of Germany. We thank the reviewers for their valuable comments.

#### References

- Bacon, C.R., Persing, H.M., Wooden, J.L., Ireland, T.R., 2000. Late Pleistocene granodiorite beneath Crater Lake caldera, Oregon, dated by ion microprobe. *Geology* 28 (5), 467–470.
- Borsato, A., Quinif, Y., Bini, A., Dublyansky, Y., 2003. Open-system alpine speleothems: implications for U-series dating and paleoclimatic reconstructions. *Studi Trentini Sci. Nat. Acta Geol.* 80, 71–83.
- Cheng, H., et al., 2013. Improvements in  $^{230}\text{Th}$  dating,  $^{230}\text{Th}$  and  $^{234}\text{U}$  half-life values, and U–Th isotopic measurements by multi-collector inductively coupled plasma mass spectrometry. *Earth Planet. Sci. Lett.* 371–372 (0), 82–91.
- Cottle, J.M., Burrows, A.J., Kylander-Clark, A., Freedman, P.A., Cohen, R.S., 2013. Enhanced sensitivity in laser ablation multi-collector inductively coupled plasma mass spectrometry. *J. Anal. Atomic Spectrom.* 28 (11), 1700–1706.
- Dorale, J., et al., 2004. Uranium-series dating of speleothems: current techniques, limits, & applications. In: Sasowsky, I., Mylroie, J. (Eds.), *Studies of Cave Sediments*. Springer, US, pp. 177–197.



- Drysdale, R.N., et al., 2012. Precise microsampling of poorly laminated speleothems for U-series dating. *Quat. Geochronol.* 14 (0), 38–47.
- Dutton, A., et al., 2009. Uplift rates defined by U-series and C-14 ages of serpulid-encrusted speleothems from submerged caves near Siracusa, Sicily (Italy). *Quat. Geochronol.* 4 (1), 2–10.
- Eggins, S.M., et al., 2005. In situ U-series dating by laser-ablation multi-collector ICPMS: new prospects for quaternary geochronology. *Quat. Sci. Rev.* 24 (23–24), 2523–2538.
- Frisia, S., Borsato, A., Fairchild, I.J., McDermott, F., Selmo, E.M., 2002. Aragonite-calcite relationships in speleothems (Grotte De Clamouse, France): environment, fabrics, and carbonate geochemistry. *J. Sediment. Res.* 72 (5), 687–699.
- Günther, D., Heinrich, C.A., 1999. Enhanced sensitivity in laser ablation-ICP mass spectrometry using helium-argon mixtures as aerosol carrier. *J. Anal. Atomic Spectrom.* 14 (9), 1363–1368.
- Hellstrom, J., 2003. Rapid and accurate uranium-series dating by MC-ICP-MS, using microdrilling and laser ablation. In: *Goldschmidt Conference Abstracts*, p. A144.
- Hoffmann, D.L., et al., 2010. Towards radiocarbon calibration beyond 28 ka using speleothems from the Bahamas. *Earth Planet. Sci. Lett.* 289 (1–2), 1–10.
- Hoffmann, D.L., et al., 2007. Procedures for accurate U and Th isotope measurements by high precision MC-ICPMS. *Int. J. Mass Spectrom.* 264 (2–3), 97–109.
- Hoffmann, D.L., Spötl, C., Mangini, A., 2009. Micromill and in situ laser ablation sampling techniques for high spatial resolution MC-ICPMS U-Th dating of carbonates. *Chem. Geol.* 259 (3–4), 253–261.
- Iizuka, T., Hirata, T., 2005. Improvements of precision and accuracy in in situ Hf isotope microanalysis of zircon using the laser ablation-MC-ICPMS technique. *Chem. Geol.* 220 (1–2), 121–137.
- Jackson, S.E., Pearson, N.J., Griffin, W.L., 2001. *Laser Ablation ICPMS in the Earth Sciences. Principles and Applications.* Mineralogical Society of Canada, St. John's, Newfoundland.
- Jochum, K.P., et al., 2012. Accurate trace element analysis of speleothems and biogenic calcium carbonates by LA-ICP-MS. *Chem. Geol.* 318–319 (0), 31–44.
- Jochum, K.P., et al., 2014. Non-matrix-matched calibration for the multi-element analysis of geological and environmental samples using 200 nm femtosecond LA-ICP-MS: a comparison with nanosecond lasers. *Geostand. Geoanal. Res.* 38 (3), 265–292.
- Jochum, K.P., et al., 2011. Determination of reference values for NIST SRM 610–617 glasses following ISO guidelines. *Geostand. Geoanal. Res.* 35 (4), 397–429.
- Kaufmann, G., 2003. Stalagmite growth and palaeo-climate: the numerical perspective. *Earth Planet. Sci. Lett.* 214 (1–2), 251–266.
- Koornneef, J.M., et al., 2012. In situ analysis of  $^{230}\text{Th}$ - $^{232}\text{Th}$ - $^{238}\text{U}$  ratios in titanite by fs-LA-MC-ICPMS. *J. Anal. Atomic Spectrom.* 27 (11), 1863–1874.
- Lachniet, M.S., Bernal, J.P., Asmerom, Y., Polyak, V., 2012. Uranium loss and aragonite-calcite age discordance in a calcitized aragonite stalagmite. *Quat. Geochronol.* 14 (0), 26–37.
- Ludwig, K.R., 2003. Mathematical-statistical treatment of data and errors for  $^{230}\text{Th}/\text{U}$  geochronology. *Rev. Mineral. Geochem.* 52 (1), 631–656.
- Mühlinghaus, C., Scholz, D., Mangini, A., 2007. Modelling stalagmite growth and  $\delta^{13}\text{C}$  as a function of drip interval and temperature. *Geochim. Cosmochim. Acta* 71 (11), 2780–2790.
- Mertz-Kraus, R., et al., 2010. In situ  $^{230}\text{Th}$ - $^{232}\text{Th}$ - $^{234}\text{U}$ - $^{238}\text{U}$  analysis of silicate glasses and carbonates using laser ablation single-collector sector-field ICP-MS. *J. Anal. Atomic Spectrom.* 25 (12), 1895–1904.
- Meyer, M.C., Cliff, R.A., Spötl, C., 2011. Speleothems and mountain uplift. *Geology* 39 (5), 447–450.
- Meyer, M.C., Cliff, R.A., Spötl, C., Knipping, M., Mangini, A., 2009. Speleothems from the earliest Quaternary: snapshots of paleoclimate and landscape evolution at the northern rim of the Alps. *Quat. Sci. Rev.* 28 (15–16), 1374–1391.
- Paul, B., et al., 2011. Melt inclusion Pb-isotope analysis by LA-MC-ICPMS: assessment of analytical performance and application to OIB genesis. *Chem. Geol.* 289 (3–4), 210–223.
- Potter, E.-K., Stirling, C.H., Wiechert, U.H., Halliday, A.N., Spötl, C., 2005. Uranium-series dating of corals in situ using laser-ablation MC-ICPMS. *Int. J. Mass Spectrom.* 240 (1), 27–35.
- Railsback, L.B., Dabous, A.A., Osmond, J.K., Fleisher, C.J., 2002. Petrographic and Geochemical screening of speleothems for U-series dating: an example from recrystallized speleothems from Wadi Sannur Cavern, Egypt. *J. Cave Karst Stud.* 64, 108–116.
- Reid, M.R., Coath, C.D., Mark Harrison, T., McKeegan, K.D., 1997. Prolonged residence times for the youngest rhyolites associated with Long Valley Caldera:  $^{230}\text{Th}$ - $^{238}\text{U}$  ion microprobe dating of young zircons. *Earth Planet. Sci. Lett.* 150 (1–2), 27–39.
- Scholz, D., Hoffmann, D.L., 2008.  $^{230}\text{Th}/\text{U}$ -dating of fossil corals and speleothems. *Quat. Sci. J.* 57, 52–76.
- Scholz, D., Hoffmann, D.L., 2011. StalAge – an algorithm designed for construction of speleothem age models. *Quat. Geochronol.* 6 (3–4), 369–382.
- Scholz, D., Hoffmann, D.L., Hellstrom, J., Bronk Ramsey, C., 2012. A comparison of different methods for speleothem age modelling. *Quat. Geochronol.* 14 (0), 94–104.
- Scholz, D. and Hoffmann, D.L., 2016, unpublished data.
- Scholz, D., et al., 2014. Diagenesis of speleothems and its effect on the accuracy of  $^{230}\text{Th}/\text{U}$ -ages. *Chem. Geol.* 387 (0), 74–86.
- Sodhi, R.N.S., 2004. Time-of-flight secondary ion mass spectrometry (TOF-SIMS): versatility in chemical and imaging surface analysis. *Analyst* 129 (6), 483–487.
- Stirling, C.H., Lee, D.C., Christensen, J.N., Halliday, A.N., 2000. High-precision in situ  $^{238}\text{U}$ - $^{234}\text{U}$ - $^{230}\text{Th}$  isotopic analysis using laser ablation multiple-collector ICPMS. *Geochim. Cosmochim. Acta* 64 (21), 3737–3750.
- Tolzmann, J., 2013. *The Reconstruction of Paleoclimate Variability in Northern Germany, during Marine Isotope Stage 5.* Johannes Gutenberg-Universität, Mainz.
- Trinquier, A., Bouman, C., Schwieters, J., Lloyd, N., 2013.  $10^{12} \Omega$  Amplifiers for High Precision Isotope Ratio Measurements of Small Sample Sizes Thermo Fisher Scientific Technical Note, 30249.
- Waight, T., Baker, J., Peate, D., 2002. Sr isotope ratio measurements by double-focusing MC-ICPMS: techniques, observations and pitfalls. *Int. J. Mass Spectrom.* 221 (3), 229–244.
- Yang, Q., et al., 2015. Lead isotope variability in speleothems—a promising new proxy for hydrological change? First results from a stalagmite from western Germany. *Chem. Geol.* 396 (0), 143–151.